Oil Slicks Classification using Multivariate Statistical Modelling Applied to SAR and PolSAR Data

Patrícia Carneiro Genovez [1]
Corina da Costa Freitas [1]
Sidnei J. S. Sant'Anna [1]
Cristina Maria Bentz[2]
João Antonio Lorenzzetti [1]

[1] Instituto Nacional de Pesquisas Espaciais - INPE
Caixa Postal 515 - 12227-010 - São José dos Campos - SP, Brasil
{genovez, corina, sidnei}@dpi.com.br; {loren}@dsr.inpe.br

[2] Centro de Pesquisas da Petrobras - CENPES
Cidade Universitária, Q.7, Ilha do Fundão – 21949-900 - Rio de Janeiro - RJ, Brasil
{cris}@petrobras.com.br

Abstract. Polarimetric Synthetic Aperture Radars (PolSAR) have been used to detect oil slicks at sea surface. The numerous platforms available, acquiring data in different formats and configurations, pose as a challenge to understand which is the better format and statistical model to improve the detection of oil. Inclusive with this issue, a combination of different data formats in a single look complex, intensity and amplitude with full and dual polarimetric channels, were evaluated in considering adequate statistical modeling to classify each data type. It was identified that the superior results were obtained by the full and dual-pol matrices, but however when the HV channel was excluded the accuracy levels were damaged. Therefore, it is better to use the data in intensity or amplitude preserving the HV channel, than to use a polarimetric data without this channel. The classifier demonstrated potential to detect the three types of oils released, being more effective in detecting biogenic oils rather than mineral oils. The uncertainty levels increase from the center to the border of the mineral oil slicks, indicating the presence of transition regions, probably related to different weathering mechanisms. Future studies should be done including more SAR images, with known occurrences and field data, to properly investigate the trade-offs related to each data format to discriminate different oil types.

Keywords: Synthetic Aperture Radar (SAR), oil slicks detection, information theory, stochastic distances, region-based classification, uncertainty maps, statistical modeling.

1. Introduction

SAR systems are the most effective and operational providers of data to detect and monitor oil spills at sea surface. These systems allow cover large areas systematically delivering data in Near Real Time (NRT). In this spectral range, oil slicks and natural phenomena known as look-alikes are detected as low backscatter regions, being identified as dark spots (Brekke & Solberg, 2005; API, 2013).

During the last decades, the launching of SAR systems increased and consolidated the systematic use of these sensors for this purpose. However, the innumerous platforms available, acquiring data in different formats with different configurations, makes the investigation about the trade-offs related with each data type needed.

Polarimetric SAR data (PolSAR) are acquired with full or dual-polarization, while Polarized SAR data are acquired with a single-polarization. Both of them can be provided preserving the amplitude and phase information through a single look complex (SLC) format, or without the phase information, through the formats in intensity or amplitude.

Satellites as Radarsat-2, RISAT-1 and Alos PalSAR-2 are able to provide full-pol data (HH-HV-VH-VV), but covering limited areas. Alos PalSAR-2, Radarsat-2, Sentinel-1, RISAT-1, TerraSAR-X and Cosmo SkyMed are able to provide dual-pol data (HH-VV; HH-VH; VV-VH). Compact or Hybrid-polarized architectures are able to emulate a full-pol data covering larger areas than those provided by the fully PolSAR systems (Paes et al., 2015; Migliaccio et al., 2015). RISAT-1 and Alos PalSAR-2 are the only systems operating, but new planned missions as Radarsat Constellation

Mission (RCM) and SAOCOM-1, will make the use of these type of data operational in a near future.

In this context, the contribution of each type of data to detect and characterize oil slicks at sea surface is a relevant topic to be investigated. The objective of this work is to evaluate the performance of the oil slicks classification combining polarization channels, different SAR data formats and considering appropriate statistical modeling.

For this purpose, a region-based classifier based on information theory and stochastic distances was applied. This classifier, named PolClass, uses a supervised approach to compare stochastic distances between statistical distributions, each one defined according to the data format evaluated. Additionally, hypothesis tests are used to associate confidence levels to the classification, providing uncertainty maps.

2. Statistical Modeling Classification Based on Stochastic Distances

The PolClass process SAR, PolSAR and optical data, using an adequate statistical modeling for different image formats. Its architecture is organized in three processing modules (Silva et al., 2013): *i*) Multivariate Amplitude: optical and SAR images in amplitude format, assumes the Multivariate Gaussian distribution; *ii*) Intensity: pair of SAR images in intensity format, assumes the multi-look Intensity-Pair distribution, and; *iii*) Polarimetric: covariance matrix in a complex format, assumes the Scaled Complex Wishart distribution.

The flowchart (Figure 1) illustrates the PolClass architecture, indicating the statistical modeling and the stochastic distances available for each module. The type of mathematical solution used - analytical or numerical - were also indicated.

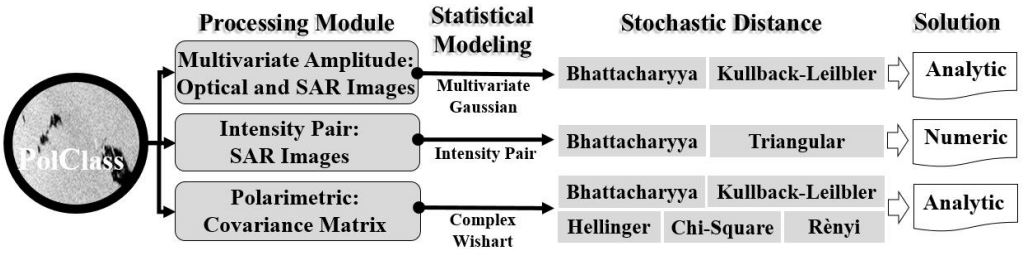

Figure 1. The PolClass architecture indicating the configuration planned for the 3 modules.

The basis to perform a region-based classification is the segmentation results, which provides S disjoint segments, $R_1,\ldots,R_S$. The data (pixels) in the segment k is denoted by Z_{ik}, with $k = 1,\ldots,S$ and $i = 1,\ldots,N_k$, where N_k is the number of pixels within the segment k.

It is important to highlight that the Z_{ik} is a matrix whereby the SAR data can be represented in a complex, intensity or amplitude format with different statistical distributions (f_x). In this way, considering that Z_{ik} follows an f_x distribution with parameter $\Sigma_k = \mathrm{E}[Z_{ik}]$, the maximum likelihood (ML) estimator of Σ_k is $\hat{\Sigma}_k = N_k^{-1} \sum_{i=1}^{N_k} Z_{ik}$.

Supposing also that the user wants to classify the image in C classes, assuming that the training samples of these classes are also f_x distributed with parameter Σ_{C_j}, with $j = 1,\ldots,C$, and that the ML estimator of Σ_{C_j} based on samples of size M_j is denoted by $\hat{\Sigma}_{C_j}$.

The objective is to classify each one of the S segments in one of the C classes. This classification is performed using stochastic distances (d_{kj}) between different statistical distributions (f_x) associated to each region R_k ($k = 1,\ldots,S$) and to each one of the training samples of class C_j. Then, using the distances calculated for each segment, a statistic of S_{kj} is used to perform statistical tests to verify the hypothesis that $\Sigma_k = \Sigma_{C_j}$ (for all i, j).

At the end of the process, the segment R_k will be assigned to a class which presents: *i*) the lower distance (d) between $\hat{\Sigma}_{C_j}$ and $\hat{\Sigma}_k$; *ii*) the lower or equivalently statistical test (S_{kj}), and a higher associated p-value p_{kj}.

The Bhattacharyya (BTC) stochastic distance was used, being the only distance available in all modules, allowing a comparative analysis. For the Polarimetric Module, the BTC distance between the Scaled Complex Wishart distributions (d_{WB}) was obtained by analytical solution, considering as parameters Σ_i and L (number of looks), as shown in equation 1 (Nascimento et al., 2012):

(1) $$d_{WB}\left(\hat{\Sigma}_k,\hat{\Sigma}_{Cj}\right)=L\left[\frac{\log\left|\hat{\Sigma}_k\right|+\log\left|\hat{\Sigma}_{C_j}\right|}{2}-\log\left|\left(\frac{\hat{\Sigma}_k^{-1}+\hat{\Sigma}_{C_j}^{-1}}{2}\right)^{-1}\right|\right]$$

For the Multivariate Amplitude Module, Theodoridis & Koutroumbas (2008) derived the BTC distance (d_{GB}) between Multivariate Gaussian distributions, being the parameters μ_i and Σ_i, as can be seen in equation 2:

(2) $$d_{GB}\left(\hat{\Sigma}_k,\hat{\Sigma}_{Cj}\right)=\frac{1}{8}\left[\left(\mu_k-\mu_{Cj}\right)\Gamma\left(\frac{\hat{\Sigma}_k+\hat{\Sigma}_{Cj}}{2}\right)^{-1}\left(\mu_k-\mu_{Cj}\right)\right]+\frac{1}{2}\log\frac{\left|\frac{\hat{\Sigma}_k+\hat{\Sigma}_{Cj}}{2}\right|}{\sqrt{\left|\hat{\Sigma}_k\right|+\left|\hat{\Sigma}_{Cj}\right|}}$$

Under the conditions stated by Frery et al. (2014) and Salicru et al. (1994), the hypothesis test $H_0:\Sigma_k=\Sigma_{C_j}$ can be performed using the statistical tests (S). The equations developed for the statistical tests between Scaled Complex Wishart distributions (S_{WB}) and between the Multivariate Gaussian distributions (S_{GB}) can be seen in the equation 3 and 4, as indicated (Silva et al., 2013):

(3) $$S_{WB}\left(\hat{\Sigma}_k,\hat{\Sigma}_{C_j}\right)=\frac{8N_kM_j}{N_k+M_j}L\left[d_{WB}\left(\hat{\Sigma}_k,\hat{\Sigma}_{C_j}\right)\right]$$

(4) $$S_{GB}\left(\hat{\Sigma}_k,\hat{\Sigma}_{C_j}\right)=\frac{N_kM_j}{N_k+M_j}\left[\left(\hat{\mu}_k-\hat{\mu}_{Cj}\right)\Gamma\left(\frac{\hat{\Sigma}_k+\hat{\Sigma}_{Cj}}{2}\right)^{-1}\left(\hat{\mu}_k-\hat{\mu}_{Cj}\right)+4\log\frac{\left|\frac{\hat{\Sigma}_k+\hat{\Sigma}_{Cj}}{2}\right|}{\sqrt{\left|\hat{\Sigma}_k\right|+\left|\hat{\Sigma}_{Cj}\right|}}\right]$$

The null hypothesis is rejected at an α significance level if the probability $\Pr\left(\chi_\nu^2>s_W\left(\hat{\Sigma}_k,\hat{\Sigma}_{C_j}\right)\right)\leq\alpha$, where χ_ν^2 represents a chi-square distribution with ν degrees of freedom, being ν the number of parameters of the statistical distribution. Independently of the distance (d) used, the classification based on a minimum test statistic consists in assigning the segment R_k to the class C_l, if $S_W\left(\hat{\Sigma}_k,\hat{\Sigma}_{C_l}\right)<S_W\left(\hat{\Sigma}_k,\hat{\Sigma}_{C_j}\right),\ \forall j\neq l$ (equation 5).

When the class C_l is assigned to the segment R_k, the p-value (p_{kl}) is calculated as $p_{kl}=\Pr\left(\chi_\nu^2>S_W\left(\hat{\Sigma}_k,\hat{\Sigma}_{C_l}\right)\right)$ (equation 6). The p-values give the uncertainties of the classification associated to each segment. Finally, at the end of the process, the classification and the uncertainty maps are provided.

Assuming homogeneous areas, Lee at al. (1994) developed an adequate statistical modeling to SAR data using pairs of images in Intensity format. This model is derived from a Bivariate Gamma distribution extracted from the Complex Whishart distribution, without a closed expression (analytical). Thus, the distance and the statistical test need an extensive and complex numerical solution, available in Silva et al. (2013).

3. SAR Data Description and Methodology

A Fine Quad-Pol Radarsat-2 image in the SLC format (Table 1) was acquired. In this occasion, three types of oils were released during an open-water-exercise promoted by the Norwegian Clean Seas Association for Operating Companies (NOFO) in the North Sea (Skrunes et al., 2014): *i*) 0.4 m^3 of plant oil to simulate false alarms caused by natural biogenic oils; *ii*) 20m^3 of emulsion containing 69% of water; *iii*) 30m^3 of crude oil.

Complementing the analysis done by Genovez et al. (2015), an evaluation about the contribution of the SAR and PolSAR data processed in different formats (complex, intensity and

amplitude) using a proper statistical modeling was proposed. The inputs needed are: *i*) the images combined with different polarizations and formats, and; *iii*) the training and the test samples.

Table 1. SAR Data Description: Radarsat-2 Fine Quad-Pol image mode.

Satellite:	Radarsat-2	**Orbit:**	Ascending	**Swath (km):**	25x25
Mode:	Fine Quad-Pol	**Polarizations:**	HH-VV-HV-VH	**Pixel Spacing (m):**	4.7 x 4.8 (Rg x Az)
Date/Time:	08/06/2011 - 17:27:53	**Incidence Angles:**	34.5°- 36.1°	**Lines x Columns:**	6307 x 3369

The VV channel in intensity was segmented using a multi-level region-growing algorithm named MultiSeg (Souza, 2005), considering as parameters: *i*) 5 levels of compression; *ii*) minimum area of 100 pixels, and; *iii*) 1dB of similarity degree, originating 923 regions.

The classification procedure considered five classes: Plant Oil (PO), Emulsion (EM), Crude Oil (CO), Vessels (VE) and Ocean (OC). The training and test samples were collected randomly, avoiding the borders where the confusion tends to be higher and sub-sampled by factor of 2 in range and azimuth directions, minimizing the spatial correlation effect.

The distances defined by equations (1) and (2), and the corresponding statistical tests (equations 3 to 4) were computed for each segment k (k = 1,…,923), and each class Cj (j = 1,…,5). As a result, two images were formed: a classified one using equation 5, and an image representing the uncertainties of the classification, using the p-values (equation 6). The flowchart at Figure 2 shows the methodology applied in this study case.

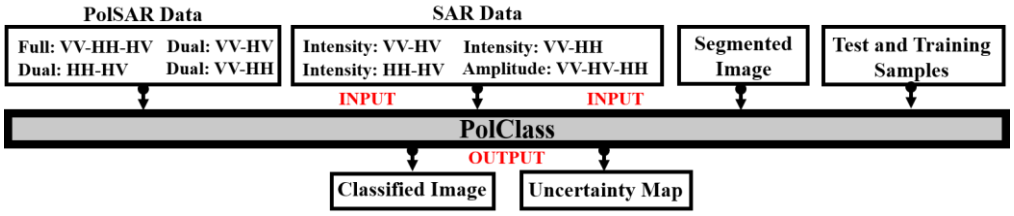

Figure 2. Methodology applied indicating the inputs and outputs of the PolClass classifier.

For the Polarimetric mode the covariance matrix is used to represent the complex data in a multi-look format and, the lexicographic outer-product matrix, to represent the data in a single-look format. In this study, the lexicographic outer-product matrices (Z) were used as input in the polarimetric mode. The matrix Z, was obtained by multiplying the scattering vector $K = [SHH, \sqrt{2}SHV, SVV]^T$ by its complex transpose (^{T}) conjugate (*) $Z = K \times K^{T*}$ (Richards, 2009).

4. Results

Figure 3 provides the classification results for all formats tested, considering different polarization channels: 3(b) SLC Full-pol; 3(c, d, e) SLC Dual-pol; 3(f, g, h) Bivariate Intensity Pairs, and; 3(i) Multivariate Amplitude.

Table 2 presents the results for the statistical tests performed to evaluate the classifications overall accuracies obtained by each format. The overall accuracies were included in the table to make the interpretation easier. Considering 95% of significance level, the overall accuracy is considered different from another when $\alpha<0.05$.

Table 2. Statistical tests done to evaluate the differences between the Overall Accuracies.

Overall Accuracy			Full-Pol	Dual-Pol			Intensity Pair			Amplitude
			HH-VV-HV	VV-HV	HH-HV	VV-HH	VV-HV	HH-HV	VV-HH	HH-HV-VV
94.87	Full-Pol	HH-VV-HV	1	0.127	0.464	0.000	0.286	0.419	0.000	0.128
95.83		VV-HV		1	0.109	0.000	0.044	0.089	0.000	0.012
94.79	Dual-Pol	HH-HV			1	0.000	0.317	0.455	0.000	0.147
84.29		VV-HH				1	0.000	0.000	0.000	0.284
94.36		VV-HV					1	0.359	0.000	0.284
94.69	Intensity	HH-HV						1	0.000	0.175
79.15		VV-HH							1	0.000
93.82	Amplitude	HH-HV-VV								1

Significance Level = 95%

Statistically Equivalent: α ≥ 0.05 — Statistically Different: α < 0.05

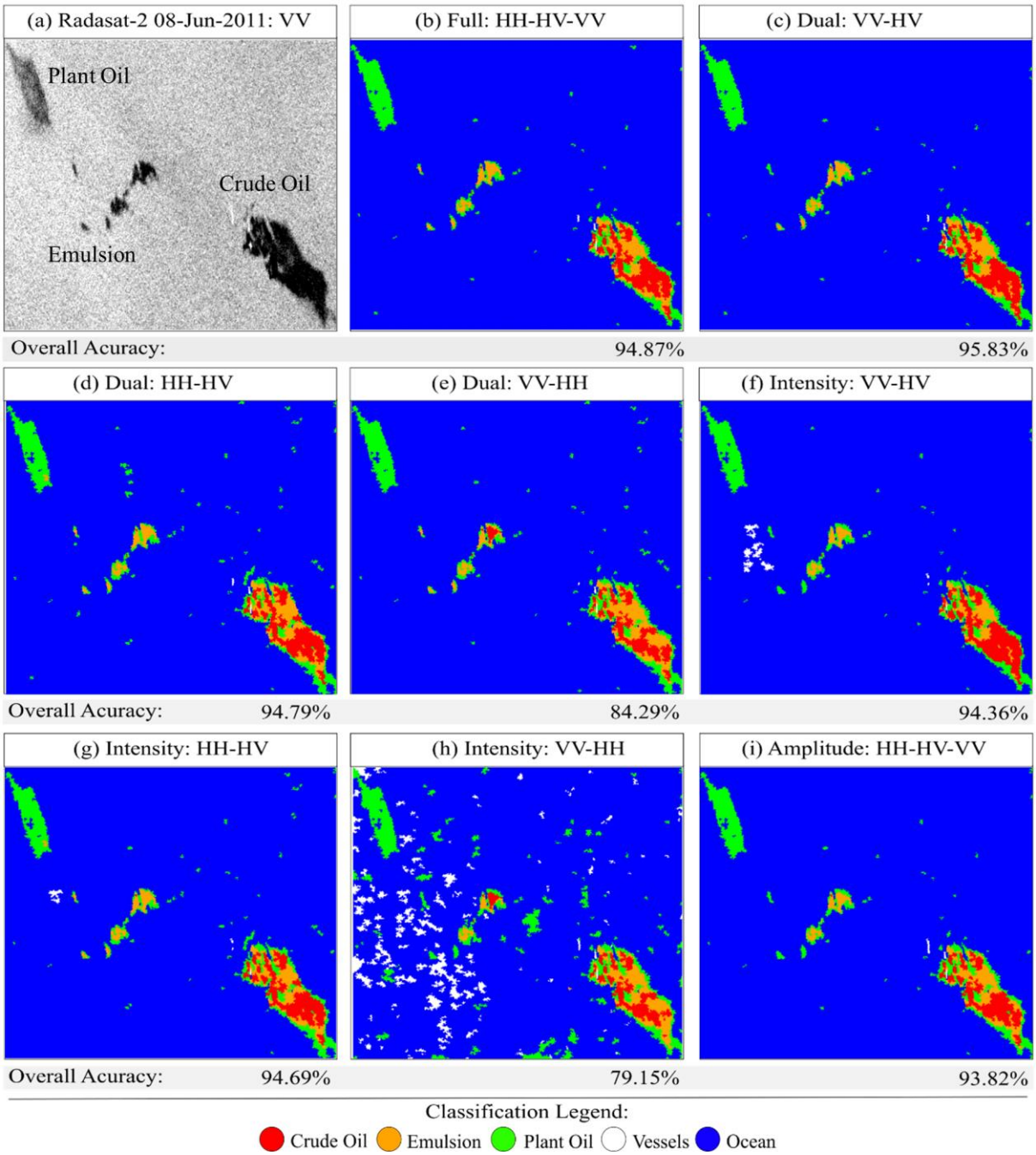

Figure 3. Classification results using the Bhattacharyya distance: (a) Radarsat-2 Scene: VV; (b) Full-pol: HH-HV-VV; (c) Dual-pol: VV-HV; (d) Dual-pol: HH-HV; (e) Dual-pol: VV-HH; (f) Intensity: VV-HV; (g) Intensity: HH-HV; (h) Intensity: VV-HH; (i) Amplitude: HH-HV-VV.

The best classification results were obtained using the dual-pol VV-HV (95.83%: Figure 3(c)) and full-pol VV-HH-HV (94.87%: Figure 3(b)) matrices, being considered statistically equivalent at 95% of confidence level (Table 2). This indicates that, in this case, using only two polarizations it is possible obtain equivalent results from that obtained using the full-polarimetric data.

The worst classification results were obtained by the data in intensity with composition VV-HH (79.15%: Fig 3(h)) and by the complex data in a dual-pol VV-HH (84.29%: Fig 3(e)). The equality tests confirmed that these formats had performances statistically different from the other results, indicating that the exclusion of the HV channel damage the classification. This can be seen in the classification map at Figure 3(h), showing in white the confusion with the VE class over the oceanic regions, and at Figure 3(e), showing the higher confusion between the classes EM and CO.

The intensity VV-HV and the dual-pol VV-HV were also considered statistically

different, thus as the dual-pol returned higher accuracy level, it is better use the data in a complex format than in intensity.

Nevertheless, considering that the dual-pol VV-HH and the intensity VV-HV are statistically different, and the overall accuracy was higher for the intensity format, it is better use the intensity format including the HV than the dual-pol without this channel. The same conclusion was valid to the comparison between intensity HH-HV and dual-pol HH-VV. In the same way, it is better use the data in amplitude HH-HV-VV including the HV channel, than in dual-pol (HH-VV) or intensity (HH-VV) excluding this channel.

The exclusion of the HV channel affected the global accuracies and, more specifically, the mineral oils detection. This can be seen in details at Figure 4, where a large portion of the EM slick was assigned as CO by the classifier (Figure 4(b, c). The reduction of the CO detection, inside of CO slick, was also observed (Figure 4(e, f).

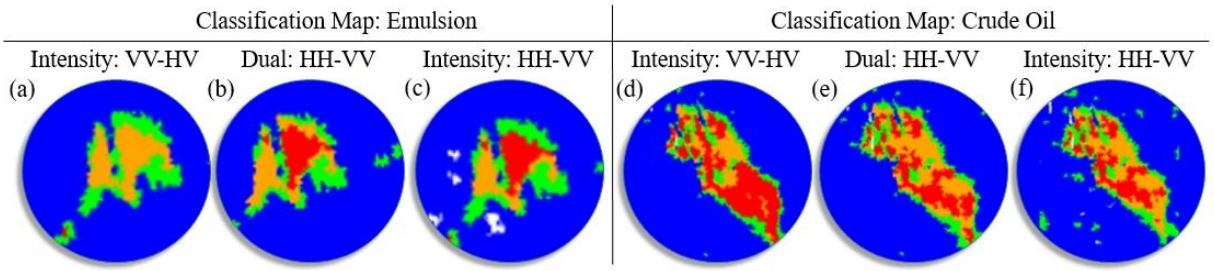

Figure 4. EM and CO details: (a, d) Intensity: VV-HV; (b, e) Dual-pol: HH-VV; (c, f) Intensity: VV-HH.

Table 3 provides: *i*) the overall accuracies; *ii*) the estimated Kappa Coefficient of Agreement; *iii*) the average of the *p*-values, and; *iv*) the percentage of segments accepted considering 99% of significance level, i.e., with *p*-values higher than 0.01.

Table 3. Assessment of Classification Results: Bhattacharyya Stochastic Distance.

	Data Format	(%) Overall Accuracy	*Kappa* ($\hat{K}$)	*P-Value Average*	(%) Accepted Segments
POLSAR	**Full: HH-HV-VV**	94.87	0.932	0.109	46.70
	Dual: VV-HV	95.83	0.944	0.087	42.47
	Dual: HH-HV	94.79	0.930	0.102	45.61
	Dual: VV-HH	84.29	0.789	0.106	43.44
SAR	**Intensity: VV-HV**	94.36	0.924	0.065	33.80
	Intensity: HH-HV	94.69	0.929	0.057	35.32
	Intensity: VV-HH	79.15	0.721	0.067	32.18
	Amplitude: HH-HV-VV	93.82	0..928	0.081	37.27

Therefore, the better accuracies were obtained by the dual-pol (VV-HV) and the full-pol (HH-HV-VV), both of them modeled with a Scaled Complex Whishart distribution. Whereby they are statistically equivalent (Table 2), the full-pol was selected to analyze the classification uncertainties. The criteria for this choice considered the higher percentage of accepted segments and the higher p-value average, reflecting higher certainties in the classification, as indicated in Table 3.

A confusion matrix (Table 4) considering all pixels of the image (Figure 3(b)) was calculated using as basis the slicks borders, designed in the Phantom mask. The supervised procedure was able to separate well all oil slicks from the ocean (96.60%: Table 4). An improved accuracy was obtained for the PO (98.46%), without confusion with mineral oils. Furthermore, the EM slick (75.4%) was better classified than the CO slick, being significantly confused with PO.

Despite the classifier had confused CO regions with the classes EM and PO, 50.87% of this slick was consistently classified with low uncertainty levels (Figure 5). Around these regions, the oil spreads generating thinner slick layers gradually (Figure 3(b)), which are recognized as EM (in orange) in some portions of the slick and as PO around its borders (in green).

Since the CO can be changed in an oil-in-water emulsion with different levels of stability, this

confusion with EM inside of the CO slick (seen in orange: Figure 3(b)) might be representing a simple confusion between classes, or a real emulsification process. The confusion with PO (in green) was observed around the EM and CO borders, which are more susceptible to the wind, currents and wave actions, inducing the spreading process.

Table 4. Confusion Matrix: Bhattacharyya distance classification using the full-pol data.

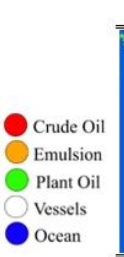

Phantom as Reference / Classification	Actual Class: EM	CO	OC	PO	VE
EM	**75.40**	36.26	0.02	0.00	0.00
CO	1.19	**50.87**	0.00	0.00	0.00
OC	0.61	0.22	**98.52**	1.54	0.00
PO	22.80	12.65	1.53	**98.46**	0.00
VE	0.00	0.00	0.01	0.00	**100**
Overall Accuracy: 96.60%					

The integrated use of the stochastic distances together with the uncertainty maps, introduced an important method to detect and analyze the oil slicks, associating confidence levels to the classification. Figure 5 provides the Bhattacharyya classification map (a) and the Uncertainty Maps: (b) Oil Slicks Uncertainty Map, and; (c) Global Uncertainty Map.

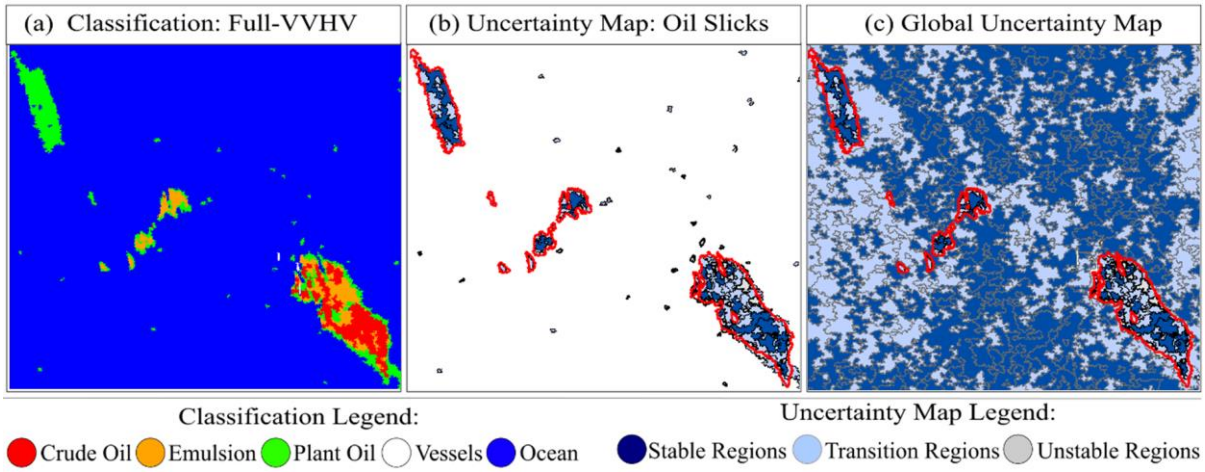

Figure 5. Bhattacharyya Classification results (a) and the uncertainty maps: (b) Oil Slicks Uncertainty Map, and; (c) Global Uncertainty Map.

The segments correctly classified and accepted by the hypothesis test characterize stable regions, reflecting with more reliability the characteristics of the assigned classes. These segments can be seen in dark blue (Figure 5(b, c)), and considering the CO and EM slick, these regions probably are related to the thicker portions of the slicks.

The segments correctly and wrongly classified but non-accepted by the hypothesis test indicate transition regions. These segments are represented in light blue Figure 5(b, c) and are concentrated around the edges and in regions where the classifier recognized different backscattering patterns. The detection of these regions, especially inside of the CO and EM slicks, may provide an indirect clue about where different weathering processes may be acting and modifying the physicochemical properties of the oils.

Finally, the accepted and wrongly classified regions are represented in grey, indicating the most instable regions, associated with a higher number of uncertainties, mainly concentrated around the borders.

5. Conclusions and Future Perspectives

The results evidenced the influence of the different SAR and PolSAR data types, with different polarization channels and statistical properties, on the classification results. As expected, the better results were obtained by the full and dual-pol matrices, however when the

HV channel is excluded the accuracy levels are damaged. Therefore, it is better use a simple data format in intensity or amplitude preserving the HV channel, than use a polarimetric data in a dual-pol composition without this channel.

Considering only the data in a full-pol format, the classifier was able to separate with high accuracy level (96.60%) the oil slicks from the ocean. It seems that the classifier detected different backscatter mechanisms within and around the crude oil and emulsion slicks, which are probably related to the weathering process, as spreading and emulsification.

The uncertainty maps interpretation allowed to identify: i) stable regions where the assignment process are more confident; ii) transition regions where the classifier might be identifying a confusion between classes or weathering processes, and; iii) unstable regions where the uncertainties in the classification are higher.

All results and conclusions obtained refer to the types of oils released, the weather and the oceanographic conditions occurring during the experiment. Future studies should be done including more SAR images with known occurrences and field data [photos and *in situ* measurements] to investigate properly the relationship between the backscatter signal, weathering stage and the thickness variations along the mineral oils.

Acknowledgments

The authors thank the Research Center of Petrobras (CENPES) for providing the Radarsat-2 data and CNPq for granting to projects #303752/2013-0 and #314248/2014-5.

6. References

API: American Petroleum Institute. Tech. Rep.: "Remote sensing in support of oil spill response: Planning guidance," API 1144, Sept, 2013.

Brekke C.; Solberg, A. H. S. "Oil spill detection by satellite remote sensing – Review," Remote Sens. Environ., vol. 95, no. 1, pp. 1–13, Mar 2005.

Frery, A. C.; Nascimento, A.D.C.; Cintra, R. J. "Analytic expressions for stochastic distances between relaxed complex Wishart distributions". *IEEE Trans. Geosci. Remote Sens.*, vol. 52, no. 2, pp. 1213–1226, 2014. DOI: 10.1109/TGRS.2013.2248737

Genovez, .P. C.; Freitas, C. C.; Sant'Anna, S.; Bentz, M. C.; Lorenzzetti, J.A. "Oil slicks detection using a polarimetric region classifier," in *Proc. IEEE Int. Geosci. Remote Sens. Symp.*, Milan – Italy, 26-31 Jul. 2015, pp. 3239 - 3242.

Lee, J. S.; Hoppel, K.W.; Mango, S. A."Intensity and phase statistics of multi–look polarimetric and interferometric SAR imagery." IEEE Transactions on Geoscience and Remote Sensing, 32, 5, 1017–1028, 1994.

Migliaccio, M.; Nunziata F.; Buono, A."SAR polarimetry for sea oil slick observation," *Int. Journal of Remote Sens.*, vol. 36, no.12, pp. 3243-3273, DOI: 10.1080/01431161.2015.1057301, 2015.

Nascimento, A. D. C. "Statistics Theory of Information for Univariate and Polarimetric Synthetic Aperture Radar Data." Ph.D. dissertation, Federal University of Pernambuco, Brazil, 2012.

Nascimento, A.D.C.; Cintra, R. J.; Frery, A. C. "Hypothesis testing in speckled data with stochastic distances," *IEEE Trans. Geosci. Remote Sens.*, vol. 48, no 1, pp. 373–385, 2010. DOI: 10.1109/TGRS. 2009.2025498

Paes, R.; Buono, A.; Nunziata, F.; Migliaccio, M.; Lorenzetti, J. A. "Compact-Polarimetry for oil basins observation," *Proc. XVII Brazilian Symposium of Remote Sensing - SBSR*, April 2015, pp. 2798-2805.

Richards, J.A. "Remote Sensing with Imaging Radar," Signals and Communication Technology, Springer. http://dx.doi.org/10.1007/978-3-642-02020-9, 2009.

Salicru, M.; Morales, D.; Menendez, M. L.; Pardo, L. "On the applications of divergence type measures in testing statistical hypotheses," *Journal of Multivariate Analysis*, vol.51, no. 2, pp. 372-391, 1994.

Skrunes, S.; Brekke, C.; Eltoft, T. "Characterization of marine surface slicks by Radarsat-2 multipolarization features," *IEEE Trans. Geosci. Remote Sens.*, vol. 52, no. 9, pp. 5302–5319, Sep. 2014.

Sousa-Junior, M. A. " Multilevel Segmentation and Multi-models for Radar and Optical Images," Ph.D. dissertation, Dept. Image Processing Division, Brazilian Institute for Space Research, São José dos Campos, São Paulo, Brazil, 2005. Available: <http://urlib.net/sid.inpe.br/jeferson/2005/06.01. 18.47>

Silva, W. B.; Freitas, C. C.; Sant'Anna, S. J. S.; Frery; A. C. "Classification of segments in PolSAR imagery by minimum stochastic distances between Wishart distributions," Journal of Selected Topics in Applied Earth Observations and Remote Sens., vol. 6,no. 3, 2013.

Theodoridis, S.; Koutroumbas, K. "Pattern Recognition," 4th. ed. San Diego, CA: Academic Press, 2008. ISBN 1597492728, 9781597492720. 26, 39